# Probe response of a cavity-optomechanical system coupling to a frequency-dependent bath

Wei Jiang,[1] Rui Yang,[1] Tian-Hui Qiu,[2] and Guo-Jian Yang[1,*]

[1]*Department of Physics, Applied Optics Beijing Area Major Laboratory, Beijing Normal University, Beijing 100875, China*

[2]*School of Science, Qingdao University of Technology, Qingdao 266520, China*

(Received 27 May 2019; revised manuscript received 22 January 2020; accepted 10 February 2020; published 4 March 2020)

We investigate the probe response of a cavity-optomechanical system with its mechanical oscillator coupling to a bosonic bath characterized by the Ohmic spectrum density. By employing the spectrum decomposition scheme, we simplify the original non-Markovian equation of motion for the system and then examine the dynamics of the intracavity field. Furthermore, we work out the probe response function and simplify it further with the linear fitting method. Based on this simplification, we obtain the details of the probe spectral profile and find that the probe response changes smoothly from the optomechanically induced transparency (OMIT) regime to the normal mode splitting regime as the driving strength increases due to the lifting of frequency degeneracy of the OMIT system by the non-Markovian effect. We also find notable probe amplification under the cavity driving resonant condition. Our method can be applied to solving a non-Markovian problem in quantum optics or other fields of physics where a bath with any frequency-dependent structure must be considered.

DOI: 10.1103/PhysRevA.101.033804

## I. INTRODUCTION

Cavity optomechanics [1,2] explores the interaction between optical modes and mechanical modes as well as relevant physical effects. With a cavity optomechanical system (OMS), one can control the mechanical response of a system by an optical field and, reversely, the optical response of a system by a mechanical or another optical field. It is this character of the cavity OMS that leads to its potential applications in ultrasensitive measurements [3–6], the quantum optical effects [7–10], and quantum information processing [11,12]. Optomechanically induced transparency (OMIT) is a typical example of light-control light via mechanical motion. The remarkable feature of the OMIT, like the well-known atomic electromagnetically induced transparency (EIT) [13,14], is the steep variation of the refractive index achieved inside the induced nonabsorptive bandwidth. Since the OMIT was first observed [15,16], successful investigations in this subject have been made, such as the OMIT-based slow-light [17,18] and ultrasensitive measurements [19–22], multicavity and hybrid OMIT [23–29], and optomechanically induced amplification (OMIA) [30–34].

The motion of a realistic mechanical oscillator is affected by its surroundings. If its oscillating frequency is much larger than the coupling strength with its environment and the correlation time of the environment is much smaller than the characteristic time of the system, the information associated with the amplitude and phase flows unilaterally via the mechanical degrees of freedom out of the system. The dynamics of the oscillator can then be described in the Born-Markovian approximation [35]. However, this approximation is not applicable when the oscillator couples strongly with a finite and frequency-dependent bath, and one may see now the flowing back of those that have flowed out, i.e., the memory effect. There is already some research progress in this aspect, including the experimental observation of non-Markovian regimes of a heat bath coupled to an OMS [36] and the theoretical demonstration of the positive role of the non-Markovian effect in the generation and preservation of the optomechanical entanglement [37,38], the cooling of the optomechanical oscillator beyond the conventional Markovian limit [39], the optomechanical force sensor [40], and the OMIA due to the non-Markovian cavity's electromagnetic reservoir [41]. In addition, the environmental engineering technique [42–45] is emerging as a promising tool for manipulating the non-Markovian environment and, therefore, the quantum dynamics of cavity OMSs, with which more secrets in this field will be declassified.

The difficulty in addressing a non-Markovian problem lies in the memory effect. Mathematically, it is a problem of how to deal with an integrodifferential equation with respect to both time and bath degrees of freedom. In a few special cases, the problem can be simplified because the spectral density of a bath has a simple form, for example, Lorentzian or Debye form, which allows the analytical calculation of integration. In this paper, we investigate the OMIT where a mechanical oscillator couples to a bosonic bath characterized by the Ohmic spectrum density. The frequency dependence of the bath and the strong enough coupling of the bath with the oscillator ensure the observable action of the non-Markovian effect. We employ the spectrum decomposition scheme (SDS) [46], which was proposed for expanding the bath correlation function required by the hierarchical equations of motion technique in solving complicated non-Markovian problems [47], to numerically fit the spectral density function with a set of analytically treatable Lorentzian functions, and then transform the original integrodifferential equation for the OMIT

*Corresponding author: yanggj@bnu.edu.cn

 ©2020 American Physical Society

system into a set of nonlinear ordinary differential equations. We examine the dynamics of the system related to the output field at frequencies of the control and probe fields, and work out the steady-state probe response function. By using the linear fitting method, we simplify this function and obtain the structure information of the probe response spectrum. We find the effective role of the non-Markovian effect in generating the OMIT effect and analyze the condition under which a notable probe amplification in the OMIT system is achieved.

The paper is organized as follows. In Sec. II, we introduce the OMIT model under consideration and work out the corresponding non-Markovian Heisenberg-Langevin equation simplified with the SDS. In Sec. III, we examine the dynamics of the intracavity fields at the frequency of the cavity mode and the probe field. Based on the result of Sec. III, we analyze in Sec. IV the steady-state probe response of our OMIT system. Section V presents our conclusions.

## II. MODEL DESCRIPTION

The model considered in this paper contains an optical Fabry-Pérot cavity with one of its mirrors acting as a mechanical oscillator of frequency $\omega_m$. The vibration mode of the oscillator is coupled with the cavity mode of frequency $\omega_c$ via radiation pressure and also with a non-Markovian environment modeled by a structured bosonic bath. The cavity mode is driven by a strong coherent field of frequency $\omega_d$, probed by a weak field of frequency $\omega_p$, and also damped by an electromagnetic reservoir. We assume that the bath is composed of an infinitive collection of independent harmonic oscillators. If operators $\hat{H}_S$, $\hat{H}_E$, and $\hat{H}_I$ are denoted as the Hamiltonians of the system, the environment, and the system plus environment, respectively, we can write the Hamiltonian of the whole model as

$$\hat{H} = \hat{H}_S + \hat{H}_E + \hat{H}_I \tag{1}$$

with

$$\begin{aligned}\hat{H}_S = {} & \hbar\omega_c \hat{a}^\dagger \hat{a} + \hbar\omega_m \hat{b}^\dagger \hat{b} - \hbar g \hat{a}^\dagger \hat{a}(\hat{b}^\dagger + \hat{b}) \\ & + i\hbar[(\varepsilon_d e^{-i\omega_d t} + \varepsilon_p e^{-i\omega_p t})\hat{a}^\dagger - \text{H.c.}],\end{aligned} \tag{2}$$

$$\hat{H}_E = \sum_k \hbar\omega_k' \hat{a}_k^\dagger \hat{a}_k + \sum_k \hbar\omega_k \hat{b}_k^\dagger \hat{b}_k, \tag{3}$$

$$\begin{aligned}\hat{H}_I = {} & \sum_k \hbar\epsilon_k'(\hat{a}_k^\dagger + \hat{a}_k)(\hat{a}^\dagger + \hat{a}) \\ & + \sum_k \hbar\epsilon_k(\hat{b}_k^\dagger + \hat{b}_k)(\hat{b}^\dagger + \hat{b}).\end{aligned} \tag{4}$$

In Eqs. (2)–(4), $\hat{a}$ ($\hat{a}^\dagger$) and $\hat{b}(\hat{b}^\dagger)$ are the annihilation (creation) operators of the cavity mode and the mechanical mode. $g$ is the oscillator-cavity coupling constant defined as $g = (\omega_c/L)\sqrt{\hbar/2m\omega_m}$ with $L$ being the cavity length and $m$ being the mass of the oscillator. $\varepsilon_d = \sqrt{2\kappa\wp_d/(\hbar\omega_d)}$ [$\varepsilon_p = \sqrt{2\kappa\wp_p/(\hbar\omega_p)}$] is the amplitudes of the strong driving (weak probe) field, where $\wp_d$ ($\wp_p$) is the driving (probe) power, and $\kappa$ is the cavity damping rate. $\hat{a}_k$ ($\hat{a}_k^\dagger$) is the annihilation (creation) operator of the reservoir for the cavity mode and $\hat{b}_k$ ($\hat{b}_k^\dagger$) is the annihilation (creation) operator of the bath for the mechanical mode. $\epsilon_k$ and $\epsilon_k'$ are the corresponding coupling constants of the reservoir with the cavity and of the bath with the oscillator, respectively.

The OMIT system fulfils Heisenberg-Langevin equations of motion. By the conventional consideration, we take the reservoir for the cavity mode as a Markovian electromagnetic vacuum, which, in the rotating-wave approximation, causes the cavity mode damping at rate $\kappa$. As to the bath for the mechanical oscillator, we assume it has a structure characterized by spectral density $J(\omega)$ defined as $\sum_k \epsilon_k^2 \delta(\omega - \omega_k) \Rightarrow \epsilon_{\omega/c}^2 \frac{dn}{d\omega} \equiv J(\omega)$ with $\frac{dn}{d\omega}$ being the bath oscillator density, and go beyond the rotating approximation with respect to the the oscillator-bath coupling. Following the textbook of quantum optics [48], from Hamiltonian Eq. (1) we can write down the formal solution of the bath operator $\hat{b}_k$

$$\dot{\hat{b}}_k(t) = \hat{b}_k(0)e^{-i\omega_k t} - i\epsilon_k \int_0^t d\tau[\hat{b}^\dagger(\tau) + \hat{b}(\tau)]e^{-i\omega_k(t-\tau)} \tag{5}$$

and, subsequently, the Heisenberg equations for the system operators $\hat{a}$ and $\hat{b}$:

$$\dot{\hat{a}} = -\left(i\Delta_c + \frac{\kappa}{2}\right)\hat{a} + ig\hat{a}(\hat{b}^\dagger + \hat{b}) + \varepsilon_d + \varepsilon_p e^{-i\delta_p t} + \sqrt{\kappa}\hat{a}_{\text{in}}, \tag{6}$$

$$\dot{\hat{b}} = -i\omega_m \hat{b} + ig\hat{a}^\dagger \hat{a} + \int_0^t d\tau K(t-\tau)[\hat{b}^\dagger(\tau) + \hat{b}(\tau)] - \xi(t), \tag{7}$$

where we have rotated the system at the frequency $\omega_d$ of the driven field. In Eqs. (6) and (7), $\Delta_c = \omega_c - \omega_d$, $\delta_p = \omega_p - \omega_d$, $\hat{a}_{\text{in}}$ is the input noise operator for the cavity mode, $K(t)$ is the integral kernel defined as $K(t) = 2i\sum_k \epsilon_k^2 \sin(\omega_k t) = 2i\int_0^\infty d\omega J(\omega)\sin(\omega t)$, and $\xi(t)$ is the bath noise operator given by $\xi(t) = i\sum_k \epsilon_k[\hat{b}_k^\dagger(0)e^{i\omega_k t} + \hat{b}_k(0)e^{-i\omega_k t}]$. Equation (7) has the time-integration term depending on the whole evolutionary history from time $t_0$ to $t$, which indicates that the dynamics of the OMIT system is of the memory effect. In the Markovian regime, this term reduces to $-\gamma_m \hat{b}$ in the rotating-wave approximation, where $\gamma_m$ is the oscillator damping rate.

Integrodifferential equation (7) is rather difficult to treat due to its double integration with respect to time $t$ and frequency $\omega$. We now employ the SDS [46] to reduce the complexity. We assume that the bath has the Ohmic spectral density $J(\omega) = \eta\omega e^{-\omega/\bar{\omega}_c}$ [49], where $\bar{\omega}_c$ is the cutoff frequency determining the position of the peak of the spectral density and $\eta$ is the dimensionless coupling strength between the oscillator and the bath. According to the SDS [46], the spectral density $J(\omega)$ can be numerically fitted with a sum of Lorentzian functions:

$$J(\omega) = \sum_{j=1}^{N} \frac{P_j \omega}{\left[(\omega + \Omega_j)^2 + \Gamma_j^2\right]\left[(\omega - \Omega_j)^2 + \Gamma_j^2\right]}. \tag{8}$$

Here $N$ is the number of Lorentzian modes required for fitting use. $\{P_j, \Omega_j, \Gamma_j\}$ ($j = 1, 2, \ldots, N$) is the set of fitting parameters for the $j$th Lorentzian mode, obtained by using the simulated annealing method [50]. Table I presents the values of $\{P_j, \Omega_j, \Gamma_j\}$, and Fig. 1 shows the comparison of the original (solid black line) with the fitted (dashed red line) spectral density lines, where a very good agreement

TABLE I. Fitting parameters in the Lorentzian-mode-decomposition scheme for the Ohmic spectral density [46].

| Ohmic | $P_j/(\eta^4\overline{\omega}_c)$ | $\Omega_j/\overline{\omega}_c$ | $\Gamma_j/\overline{\omega}_c$ |
|---|---|---|---|
| 1 | 12.0677 | 0.2378 | 2.2593 |
| 2 | −19.9762 | 0.0888 | 5.4377 |
| 3 | 0.1834 | 0.0482 | 0.8099 |

over the whole range of frequency can be seen. Replacing $J(\omega)$ in the integral kernel $K(t)$ with its decomposition (8) and finishing the integration over the bath frequencies, we transform Eq. (7) into

$$\dot{\hat{b}} = -i\omega_m\hat{b} + ig\hat{a}^\dagger\hat{a} + \sum_j \frac{iP_j\pi}{2\Omega_j\Gamma_j}\int_0^t d\tau e^{-\Gamma_j(t-\tau)} \times \sin[\Omega_j(t-\tau)][\hat{b}^\dagger(\tau)+\hat{b}(\tau)] - \xi(t), \tag{9}$$

with which our further analysis can be simplified.

## III. NON-MARKOVIAN DYNAMICS OF THE OMIT SYSTEM

In this section, we examine the non-Markovian dynamics of the OMIT system. Similar to the atomic EIT [13,14], the OMIT is the phenomenon of mean response of the cavity optomechanical system to the probe field in the presence of the driving field. This means that the quantum fluctuations are not under consideration and thus the factorization assumption $\langle\hat{A}\hat{B}\rangle = \langle\hat{A}\rangle\langle\hat{B}\rangle$ is reasonable. We focus on three main components of the intracavity field, which, in the original frame, oscillate at frequencies $\omega_d$, $\omega_p$, and $2\omega_d-\omega_p$, and obtain them from the following expansion:

$$\langle\hat{Q}\rangle(t) = Q_0(t) + Q_+(t)\varepsilon_p e^{-i\delta_p t} + Q_-(t)\varepsilon_p^* e^{i\delta_p t}, \tag{10}$$

where $\langle\hat{Q}\rangle(t)$ stands for the expectation of operator $\hat{Q}$ ($\hat{Q}=\hat{a},\hat{b}$), and $Q_\sigma(t)$ ($Q_\sigma = a_\sigma, b_\sigma$, with subscripts $\sigma = 0,+,-$ referring, respectively, to the above three frequencies) is the time-dependent coefficient of the $\sigma$ component. Substituting Eq. (10) into both sides of Eqs. (6) and (9) in their mean value forms, dropping the terms that contain the products of more than one small quantity $\varepsilon_p$, and finally equating coefficients of terms with the same frequency, we derive the following equations of motion for $Q_\sigma(t)$:

$$\begin{aligned}
\dot{a}_0 &= -\Big(i\Delta_c + \frac{\kappa}{2}\Big)a_0 + iga_0(b_0^*+b_0) + \varepsilon_c a_0,\\
\dot{b}_0 &= -i\omega_m b_0 + iga_0a_0^* - \sum_j\big[\theta_{01}^{(j)} + \theta_{02}^{(j)}\big],\\
\dot{\theta}_{01}^{(j)} &= -(\Gamma_j + i\Omega_j)\theta_{01}^{(j)} + 2I_j(b_0^*+b_0),\\
\dot{\theta}_{02}^{(j)} &= -(\Gamma_j - i\Omega_j)\theta_{02}^{(j)} - 2I_j(b_0^*+b_0),
\end{aligned} \tag{11}$$

with the definition

$$\begin{aligned}
\theta_{01}^{(j)}(t) &= \int_0^t d\tau\frac{P_j\pi}{4\Omega_j\Gamma_j}e^{-\Gamma_j(t-\tau)}e^{-i\Omega_j(t-\tau)}[b_0^*(\tau)+b_0(\tau)],\\
\theta_{02}^{(j)}(t) &= -\int_0^t d\tau\frac{P_j\pi}{4\Omega_j\Gamma_j}e^{-\Gamma_j(t-\tau)}e^{i\Omega_j(t-\tau)}[b_0^*(\tau)+b_0(\tau)],
\end{aligned} \tag{12}$$

and

$$\begin{aligned}
\dot{a}_+ &= \Big(i\delta_p - i\Delta_c - \frac{\kappa}{2}\Big)a_+ + 1\\
&\quad + ig(a_0b_+ + b_0a_+ + a_0b_-^* + b_0^*a_+),\\
\dot{b}_+ &= i(\delta_p-\omega_m)b_+ + ig(a_0^*a_+ + a_0a_+^*)\\
&\quad - \sum_j\big[\theta_{+1}^{(j)} + \theta_{+2}^{(j)}\big],\\
\dot{a}_-^* &= \Big(i\delta_p + i\Delta_c - \frac{\kappa}{2}\Big)a_-^*\\
&\quad - ig(a_0^*b_+ + b_0a_-^* + a_0^*b_-^* + b_0^*a_-^*),\\
\dot{b}_-^* &= i(\delta_p+\omega_m)b_-^* - ig(a_0^*a_+ + a_0a_-^*)\\
&\quad + \sum_j\big[\theta_{+1}^{(j)} + \theta_{+2}^{(j)}\big],\\
\dot{\theta}_{+1}^{(j)} &= [i\delta_p - (\Gamma_j + i\Omega_j)]\theta_{+1}^{(j)} + 2I_j(b_-^*+b_+),\\
\dot{\theta}_{+2}^{(j)} &= [i\delta_p - (\Gamma_j - i\Omega_j)]\theta_{+2}^{(j)} - 2I_j(b_-^*+b_+),
\end{aligned} \tag{13}$$

with the definition

$$\begin{aligned}
\theta_{+1}^{(j)}(t) &= \int_0^t d\tau\frac{P_j\pi}{4\Omega_j\Gamma_j}e^{-\Gamma_j(t-\tau)}e^{-i(\Omega_j-\delta_p)(t-\tau)}\\
&\quad\times[b_0^*(\tau)+b_0(\tau)],\\
\theta_{+2}^{(j)}(t) &= -\int_0^t d\tau\frac{P_j\pi}{4\Omega_j\Gamma_j}e^{-\Gamma_j(t-\tau)}e^{i(\Omega_j+\delta_p)(t-\tau)}\\
&\quad\times[b_0^*(\tau)+b_0(\tau)],
\end{aligned} \tag{14}$$

and $I_j = \frac{P_j\pi}{8\Omega_j\Gamma_j}$. The memory effect of the bath comes into the OMIT dynamics through the time-dependent behavior of $\theta_{\sigma 1}^{(j)}$ and $\theta_{\sigma 2}^{(j)}$ ($\sigma = 0,+,-$). Substituting Eq. (12) into the equation on the second line of Eq. (11), we arrive at the equations of motion for the expectations of operators $\hat{a}$ and $\hat{b}$, which are exactly the same as those obtained when we make the expectation and factorization about Eqs. (6) and (7) in the absence of the probe field. Equation (13) is not closed because the time-dependent quantities $a_0$ and $b_0$ are involved in the dynamics of quantities, $a_\pm$ and $b_\pm$.

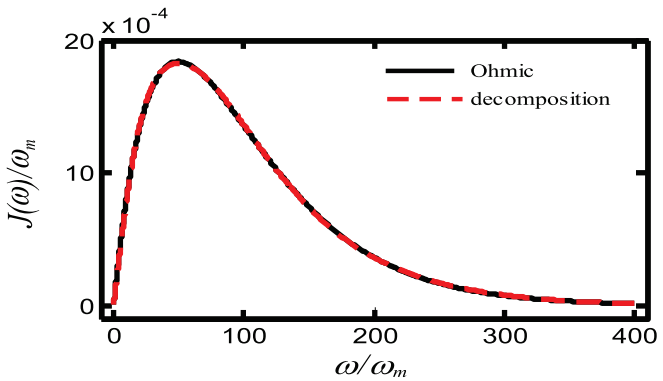


FIG. 1. Comparison of Ohmic spectral density (solid black line) with its Lorentzian-mode decomposition (dashed red line) based on Eq. (8) [46].

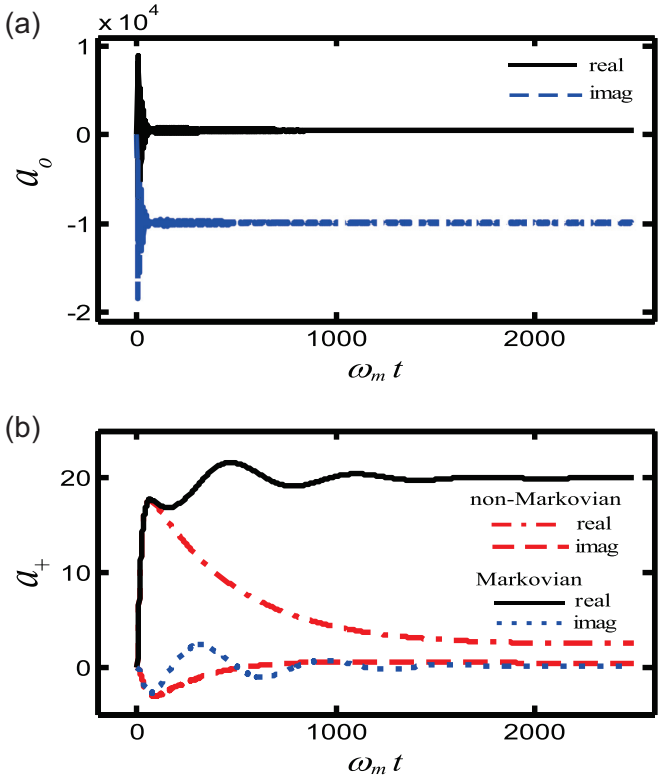


FIG. 2. Time evolution of the (a) $\omega_d$ component and (b) $\omega_p$ component of the output field based on Eqs. (11)–(14). The parameters are $\varepsilon_d/\omega_m = 10^4$, $\Delta_c/\omega_m = 1.0$, $\delta_p/\omega_m = 0.991$, $g/\omega_m = 10^{-5}$, $\kappa/\omega_m = 0.1$, $\bar{\omega}_c/\omega_m = 50$, and $\eta = 10^{-4}$, and in the Markovian case $\gamma_m/\omega_m = 9.8 \times 10^{-5}$. The three sets of spectral decomposition parameters, $\{P_j, \Omega_j, \Gamma_j\}$ for $j = 1, 2, 3$, come from Table I.

The OMIT is an optical effect that occurs in the steady state. By employing the linear stability analysis about Eqs. (11) and (13), we can obtain the parametric region for the stable solutions. On the other hand, the memory effect is unique to a non-Markovian system. The memory time can be estimated in terms of the correlation time of the bath's noise operators $\xi(t)$, determined by the structure parameter $\bar{\omega}_c$ of $J(\omega)$ in the case of the Ohmic spectrum density. In addition, coupling constant $\eta$ must be large enough so that the memory effect can be detected. In Fig. 2 we show the result with the set of parameters in the range obtainable with experimental techniques [51]: $\lambda = 1064$ nm, $\wp_d = 3.32$ mW, $\omega_m = 2\pi \times 800$ kHz, $m = 145$ ng, $L = 10.0$ mm, $\kappa = 2\pi \times 80$ kHz, $\Delta_c/\omega_m = 1.0$, $\delta_p/\omega_m = 0.99$, $\eta = 10^{-4}$, and $\bar{\omega}_c = 2\pi \times 40$ MHz [49]. From these parameters, we can obtain scaled parameters in the equations above: $g/\omega_m = 10^{-5}$, $\varepsilon_d/\omega_m = 10^4$, $\kappa/\omega_m = 0.1$, and $\bar{\omega}_c/\omega_m = 50$. The three sets of spectral decomposition parameters, $\{P_j, \Omega_j, \Gamma_j\}$ for $j = 1, 2, 3$, come from Fig. 1. The corresponding memory time is about $\omega_m t = 0.15$, which already approaches the characteristic time of the oscillator and is thus long enough to interfere with the dynamics of the OMIT system. We note here that all figures in the rest of this paper are plotted with the parameters, if no specific declaration is made, that come from Figs. 1 and 2. Figure 2(a) shows the time evolution of the real part of the $\omega_d$ component of the intracavity optical field and its imaginary part. Figure 2(b) is devoted to the $\omega_p$ component of the intracavity optical field. It is seen that after the transitional process is over the equilibrium is built up between the OMIT system and its surroundings, and thus the system reaches the steady state. By comparison, Fig. 2(b) also presents the $\omega_p$ component as the system works in the Markovian approximation, where the decay rate $\gamma_m$ of the oscillator is decided based on $\gamma_m = \sum_k \epsilon_k^2 \delta(\omega_m - \omega_k) = \eta\omega_m e^{-\omega_m/\bar{\omega}_c}$ [49], and thus $\gamma_m/\omega_m = 9.8 \times 10^{-4}$. It is seen that under this set of parametric conditions the non-Markovian effect brings about the probe absorption of the $\omega_p$ component in the steady state much less than the Markovian one. We find that the coupling strength $\eta$ is an important parameter, which determines not only the non-Markovian effect but also the stability of the OMIT system. For instance, under the condition that other parameters above are unchanged, the system will lose its stability if $\eta > 0.005$.

## IV. PROBE RESPONSE WITH NON-MARKOVIAN EFFECT

The output probe response of the OMIT system in the frequency domain can be known from the steady-state solution of Eqs. (11)–(13) through $\mathcal{E}_T = \kappa a_+$, the output field at frequency $\omega_p$. From the real part of $\mathcal{E}_T$, $\mathrm{Re}(\mathcal{E}_T)$, and its imaginary part $\mathrm{Im}(\mathcal{E}_T)$, we obtain its absorption and dispersion, respectively. $\mathcal{E}_T$ can be rewritten as $\mathcal{E}_T = \mathcal{E}_+ + \mathcal{E}_-$ as the function of $x = \delta_p - \omega_m$ (see the Appendix for details), i.e.,

$$\mathcal{E}_\pm = \frac{1}{2(x - x_\pm)} \zeta_1(x) \left\{ i \pm \zeta_2(x) [8\beta - \zeta_2(x)^2]^{-\frac{1}{2}} \right\}, \quad (15)$$

$$x_\pm = -\frac{i}{2}[\kappa + i2(\Delta - \omega_m) - \zeta_2(x)] \pm \frac{1}{2}[8\beta - \zeta_2(x)^2]^{\frac{1}{2}}, \quad (16)$$

where $x_\pm$ is the complex eigenfrequencies of the OMIT system [16,52] and derived from the denominator of $\mathcal{E}_T(x)$, with their real parts $\mathrm{Re}(x_\pm)$ being the frequencies of transmission modes "±" and their imaginary parts $\mathrm{Im}(x_\pm)$ being the linewidths. The functions $\zeta_i(x)$ $(i = 1, 2)$ in Eqs. (15) and (16) are defined as

$$\zeta_1(x) = 1 - \frac{2i\omega_m\beta}{[x^2 + 2\omega_m x + \omega_m \chi(x)]\left(\frac{\kappa}{2} - ix - i\Delta - i\omega_m\right)}, \quad (17)$$

$$\zeta_2(x) = \frac{\kappa}{2} + i(\Delta - \omega_m) - i\frac{\chi(x)}{2}, \quad (18)$$

$$\chi(x) = \phi(x)\left(1 + \frac{\omega_m}{\Delta} + \frac{i\kappa}{2\Delta}\right) + \frac{1}{\Delta}\left(2\omega_m + \frac{i\kappa}{2} + \phi(x)\right)x + \left(\frac{1}{\omega_m} + \frac{3}{\Delta} + \frac{i\kappa}{2\omega_m\Delta}\right)x^2 + \frac{1}{\omega_m\Delta}x^3, \quad (19)$$

$$\phi(x) = \sum_j \frac{\pi P_j \omega_m}{\left\{\Omega_j^2 + [\Gamma_j - i(x - \omega_m)]^2\right\}\Gamma_j}, \quad (20)$$

where $\beta$ is propositional to the driving strength $\varepsilon_d$ and $\Delta$ is the cavity detuning modified by the mechanical motion.

Because the denominator of Eq. (15) is a high-order function of $x$, and $\mathcal{E}_+$ $(x_+)$ is not a complex conjugate of $\mathcal{E}_-$ $(x_-)$,

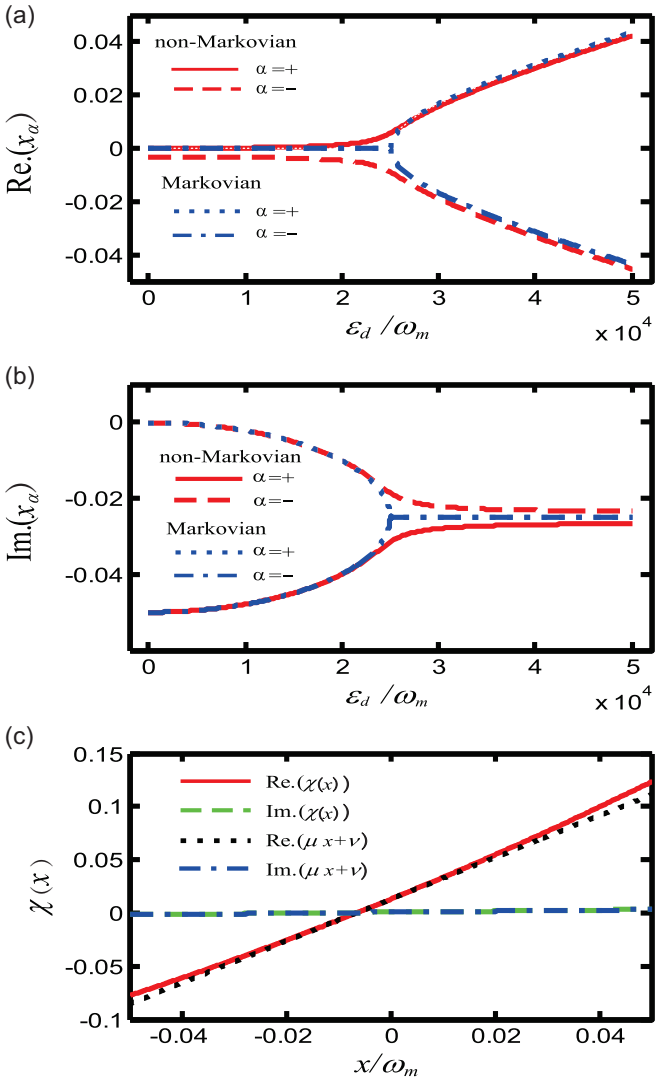


FIG. 3. (a) Plots of $\mathrm{Re}(x_\alpha)$ and (b) plots of $\mathrm{Im}(x_\alpha)$ ($\alpha = +, -$) via $\varepsilon_d$ in both Markovian and non-Markovian cases, where the $x$ coordinate, $\bar{\varepsilon}_d$, of point $o$ is the critical driving strength. (c) Plots of $\mathrm{Re}[\chi(x)]$ and $\mathrm{Im}[\chi(x)]$ fulfilling Eq. (19) and of linear fitting $\mathrm{Re}(\mu x + \nu)$, $\mathrm{Im}(\mu x + \nu)$ with $\mu = 1.9663 + 0.1i$ and $\nu/\omega_m = 1.25 \times 10^{-2} + 7 \times 10^{-4} i$. Parameters are the same as Fig. 2.

the non-Markovian probe response spectrum may display in general an asymmetric multipeak structure, where each peak represents an eigenmode with frequency equal to the peak location $\mathrm{Re}(x_\alpha)$ on the $x$ axis and with the linewidth equal to the peak width $\mathrm{Im}(x_\alpha)$. The following analysis is devoted to the probe response in the range of the OMIT parameters. First, let us recall the Markovian result. In this case, the OMIT appears at the two-photon resonant point $\delta_p = \omega_m$ and $\Delta \simeq \omega_m$, and $\mathcal{E}_\pm$ gives rise to a two-peak spectrum. And $x_\pm$ can be obtained analytically [15,16]. The dotted and dash-dotted black lines for $\mathrm{Re}(x_\pm)$ in Fig. 3(a) and for $\mathrm{Im}(x_\pm)$ in Fig. 3(b) show the locations and widths of peaks "±" as the function of the driving strength $\varepsilon_d$, respectively. There is a critical driving strength $\bar{\varepsilon}_d$. If $\varepsilon_d < \bar{\varepsilon}_d$, the OMIT arises due to destructive interference between the intracavity probe photon and anti-Stokes photon of the intracavity driving field, with the transparency window in the transmission spectrum centering at the resonant point $\mathrm{Re}(x_\pm) = 0$ and opening with the width $\mathrm{Im}(x_-)$ due to $\mathrm{Re}(\mathcal{E}_-) < 0$. If $\varepsilon_d > \bar{\varepsilon}_d$, the probe response enters the normal mode splitting (NMS) regime [53] originating from the lifting of the frequency degeneracy of the two resonant modes, i.e., $\mathrm{Re}(x_+) \neq \mathrm{Re}(x_-)$, due to the strong driving field, where the absorption peaks separate a distance proportional to the driving strength, but have a common fixed width [15,16].

In the non-Markovian case, it is impossible to derive the analytical expression of $x_\pm$ directly. As shown by Fig. 3(c) for the parameters coming from Fig. 2, the complex function $\chi(x)$ at $\delta_p = \omega_m \simeq \Delta$ varies slowly in $x$, and thus we can make a linear fitting for it, i.e., $\chi(x) = \mu x + \nu$ with complex fitting coefficients $\mu$ $(=1.9663 + 0.1i)$ and

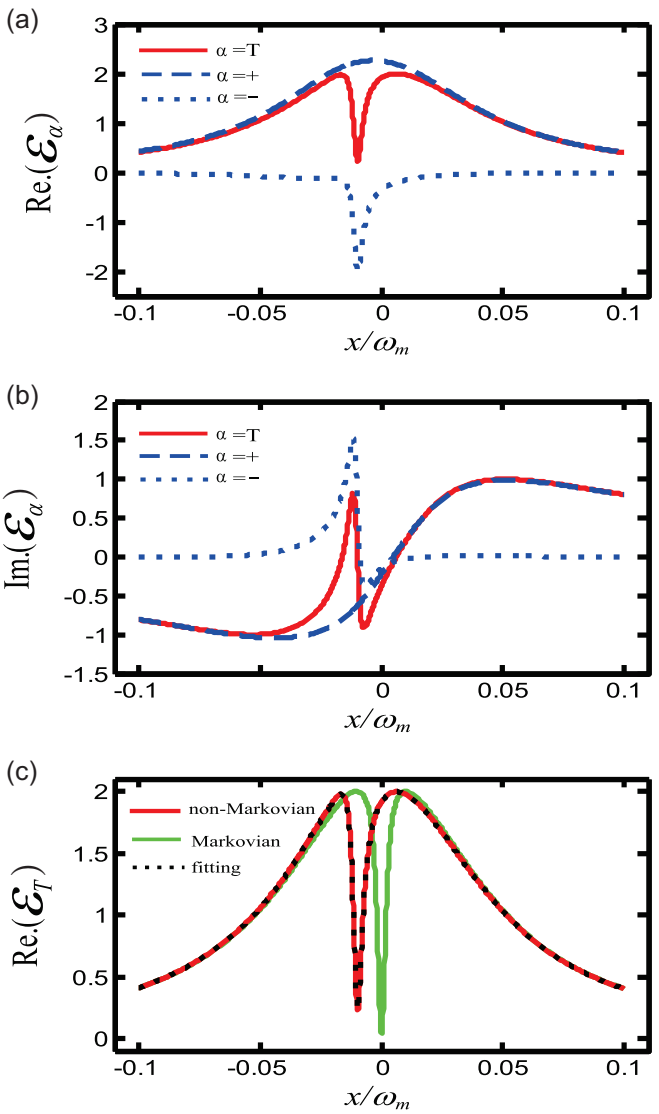


FIG. 4. Plots of (a) $\mathrm{Re}(\mathcal{E}_\alpha)$ and (b) $\mathrm{Im}(\mathcal{E}_\alpha)$ with solid red, dashed blue, and dotted blue lines corresponding to $\mathcal{E}_\alpha$ $(\alpha = T, +, -)$, respectively, and (c) $\mathrm{Re}(\mathcal{E}_T)$ obtained based on (15) and (16) (solid red line), linear fitting based on (15) and (21) (dotted black line), and Markovian result (solid green line). The parameters are the same as Fig. 2.

$\nu$ [$= (1.25 \times 10^{-2} + 7 \times 10^{-4} i)\omega_m$]. Then, inserting the linear expression of $\chi(x)$ into the denominator of Eq. (15), we derive the analytical expression of $x_\pm$:

$$x_\pm = -\frac{i}{2}\left[\frac{\kappa}{2} - i\rho \pm \sqrt{\left(\frac{\kappa}{2} + i\rho\right)^2 - 16\beta\rho/\nu}\right], \qquad (21)$$

where $\rho$ is a complex constant defined as $\rho = \nu/(2+\mu)$. If $-i\rho$ is replaced with $\gamma_m$, i.e., $\mu = 0.0$ and $-i\nu = \gamma_m$, Eq. (21) returns to its Markovian counterpart [16]. Obviously, two transmission peaks are always separated by a distance $\mathrm{Im}\sqrt{(\kappa/2 + i\rho)^2 - 16\beta\rho/\nu}$. This distance starts at $\mathrm{Re}(-\rho)$ in the weak driving limit ($\varepsilon_d = 0$) and ends with $4\mathrm{Im}[\beta/(2+\mu)]^{1/2}$ in the leading order of the strong driving. Thus, there is no transition driving strength that can serve as a distinct boundary between the OMIT and the NMS regimes. The solid and dashed red lines in Figs. 3(a) and 3(b) are plotted based on Eq. (21) and show $\mathrm{Re}(x_\pm)$ and $\mathrm{Im}(x_\pm)$ as the function of driving strength $\varepsilon_d$, respectively, from which we can see that the probe response changes smoothly from the OMIT regime to the NMS regime as the driving strength increases. Relatively, in the OMIT regime, the absorptive peak locations change with respect to the Markovian results more evidently than the peak widths do, while in the NMS regime these peaks behave oppositely. The observation above is attributed to the fact that the non-Markovian effect lifts the frequency degeneracy of the system although it operates in the OMIT regime, so that the connection of the OMIT with the NMS regimes becomes smooth.

Figure 4 is plotted based on Eqs. (15) and (21), describing in Fig. 4(a) the probe absorption spectrum $\mathrm{Re}(\mathcal{E}_T)$, being the sum of $\mathrm{Re}(\mathcal{E}_+)$ and $\mathrm{Re}(\mathcal{E}_-)$; in Fig. 4(b) its probe dispersion partner $\mathrm{Im}(\mathcal{E}_\alpha)$; and in Fig. 4(c) the comparison between the Markovian and non-Markovian results. We can see all the features of the non-Markovian OMIT predicted from Fig. 3(a) and its OMIT dispersion inside the transparency window. However, the window is not totally transparent due to the surplus absorption after the asymmetric OMIT destructive interference. We note here that in Fig. 4(c) the original spectrum obtained based on Eqs. (15) and (16) (solid red line) overlaps perfectly with that based on Eqs. (15) and (21) obtained by linear fitting for $\chi(x)$ (dotted black line). Thus, for the non-Markovian OMIT analysis, the treatment simplified by the linear fitting for $\chi(x)$ is sufficiently precise. Figure 5 focuses on the case of strong driving ($\varepsilon_d/\omega_m = 10^5$) in the NMS regime. As expected from Eq. (21), the strong driving field enlarges the transparency region between the two NMS absorptive peaks (see peaks 1-1′ from the solid red line for $\eta = 10^{-4}$). Interestingly, the strong oscillator-bath coupling widens this region further (see peaks 2-2′ from the dotted green line for $\eta = 10^{-3}$).

The OMIA is the phenomenon of negative probe absorption that occurs due to constructive interference of the intracavity probe field with the Stokes sideband of the intracavity driving field when the driving field is resonant with the motion blue sideband of the cavity, i.e., when $\Delta_c = -\omega_m$ [31]. In the present model, we observe this phenomenon even as the driving field is resonant with the cavity mode. Figure 6 is plotted based on Eqs. (15) and (21) for $\Delta_c = 0$. The $\mathrm{Re}(\mathcal{E}_T)$ spectrum now displays a four-peak structure,

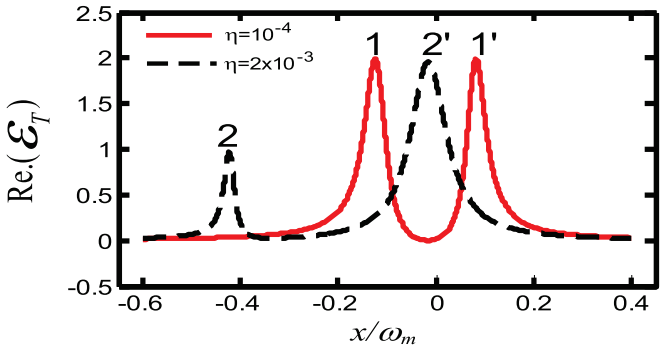


FIG. 5. Plot of $\mathrm{Re}(\mathcal{E}_T)$ for $\varepsilon_d/\omega_m = 10^5$, $\eta = 10^{-4}$ (solid red line), and $\eta = 2 \times 10^{-3}$ (dashed blue line). All other parameters are the same as Fig. 2.

where the downward peaks mean the probe amplification and, as shown by Fig. 6(b), each peak centers at the point satisfying $x - \mathrm{Re}(x_\alpha) = 0$. A notable feature is a pair of sharp amplification-absorption peaks 1-4 residing symmetrically at $x \simeq -2\omega_m$, 0, or $\delta_p \approx \pm\omega_m$. Under the present parametric condition, the amplification peak at $\delta_p \approx \omega_m$ can be observed as $\Delta_c$ takes the value in the range of $|\Delta_c| \leqslant 0.23\omega_m$. The OMIA for the small cavity detuning may be considered as the result of constructive interference of the intracavity probe field with the intracavity anti-Stokes sideband of the driving field, assisted by the resonantly excited cavity mode. On the other hand, coupling to the frequency-dependent bath leads to the

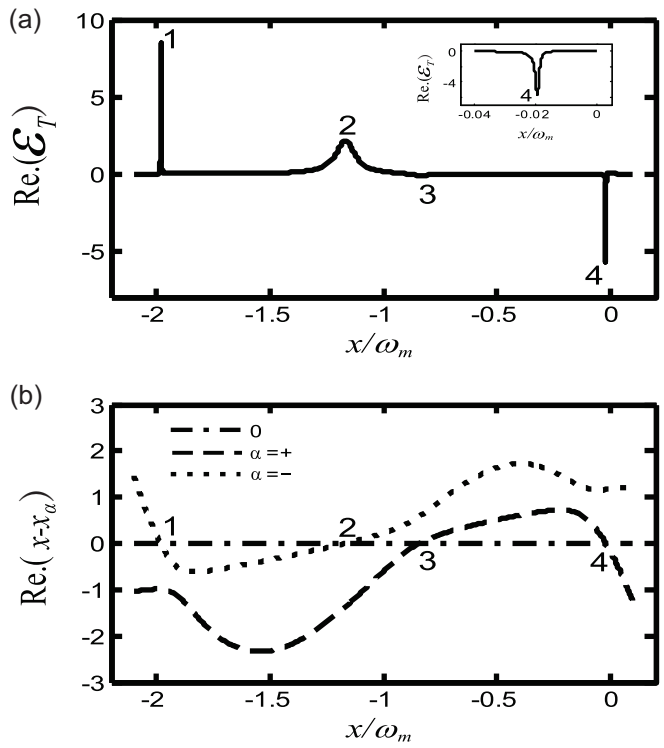


FIG. 6. (a) Plot of $\mathrm{Re}(\mathcal{E}_T)$ for $\Delta_c = 0$. The inset presents the horizontally enlarged view centering at $x \simeq 0$ ($\delta_p \simeq -\omega_m$). (b) Plot of $x - \mathrm{Re}.(x_\alpha)$ via $x$ for $\alpha = +$ (dashed line) and $\alpha = -$ (dotted line). The peaks in (a) reside at $x$ fulfilling $x - \mathrm{Re}.(x_\alpha) = 0$. All other parameters are the same as Fig. 2.

dynamics of the oscillator with the memory effect and thus to a complicated time-dependent decay behavior, which may result in the modifications of the characteristic frequencies of the system and their linewidths. The above memory effect comes into effect through the radiation-pressure coupling between the oscillator and the optical mode, and increases the adjustable ranges of the control parameters for the optical response of interest.

## V. CONCLUSION

In conclusion, we have investigated the influence of the non-Markovian effect on the OMIT where the mechanical oscillator couples a bath characterized by the Ohmic spectral density. With the help of the SDS, we transformed the original integrodifferential equation for the OMIT system into a set of ordinary differential equations, which allows us to easily carry out the stability analysis and the discussion about the steady-state optical response of the OMIT system under the influence of the non-Markovian effect. The probe absorptive spectrum might have a multipeak structure and the linear fitting treatment makes its details obtainable analytically. We found that the non-Markovian effect leads to the smooth transition of the probe response from the OMIT regime to the NMS regime as the driving strength increases. A notable probe amplification appears due to constructive interference of the intracavity probe field with the Stokes sideband of the intracavity driving field. Our method can be applied to solving a non-Markovian problem where a bath with any frequency-dependent structure must be considered.

## ACKNOWLEDGMENTS

This work was supported by National Natural Science Foundation of China under Grants No. 11654003, No. 11174040, and No. 11604174; Fundamental Research Funds for the Central Universities (Grant No. 2017TZ01); and Interdisciplinary Research Funds of Beijing Normal University.

## APPENDIX: INTRACAVITY FIELD AT PROBE FREQUENCY

The intracavity field at probe frequency $\omega_p$ fulfils Eqs. (11)–(13) and in steady state reads

$$a_+ = \frac{\left(\delta^2 - \omega_m^2 + \phi\right)\left[\frac{\kappa}{2} - i(\delta + \Delta)\right] - 2i\omega_m\beta}{\left(\delta^2 - \omega_m^2 + \phi\right)\left[(\frac{\kappa}{2} - i\delta)^2 + \Delta^2\right] + 4\omega_m\Delta\beta} \tag{A1}$$

with

$$\begin{aligned}
\varphi &= -\sum_j \frac{\pi P_j}{\left(\Omega_j^2 + \Gamma_j^2\right)\Gamma_j}, \\
\phi &= \sum_j \frac{\pi P_j \omega_m}{\left[\Omega_j^2 + (\Gamma_j - i\delta)^2\right]\Gamma_j}, \\
\beta &= g^2|a_0|^2, \\
\Delta &= \Delta_c - \frac{2\beta}{\omega_m + \varphi}, \\
a_0 &= \frac{\varepsilon_d}{i\Delta + \frac{\kappa}{2}}.
\end{aligned} \tag{A2}$$

[1] P. Meystre, Ann. Phys. (Berlin) **525**, 215 (2013).
[2] M. Aspelmeyer, T. J. Kippenberg, and F. Marquardt, Rev. Mod. Phys. **86**, 1391 (2014).
[3] P. Verlot, A. Tavernarakis, T. Briant, P.-F. Cohadon, and A. Heidmann, Phys. Rev. Lett. **104**, 133602 (2010).
[4] S. Kolkowitz, A. C. Bleszynski Jayich, Q. P. Unterreithmeier, S. D. Bennett, P. Rabl, J. G. E. Harris, and M. D. Lukin, Science **335**, 1603 (2012).
[5] S. Barzanjeh, S. Guha, C. Weedbrook, D. Vitali, J. H. Shapiro, and S. Pirandola, Phys. Rev. Lett. **114**, 080503 (2015).
[6] Y. Y. Zhi, X. C. Yu, H. J. Chen, B. O. Guan, and Y. F. Xiao, Opt. Lett. **44**, 2426 (2019).
[7] L. Tian, Phys. Rev. Lett. **108**, 153604 (2012).
[8] L. Tian, Phys. Rev. Lett. **110**, 233602 (2013).
[9] Y. C. Liu, Y. F. Xiao, Y. L. Chen, X. C. Yu, and Q. H. Gong, Phys. Rev. Lett. **111**, 083601 (2013).
[10] X. X. Ren, H. K. Li, M. Y. Yan, Y. C. Liu, Y. F. Xiao, and Q. H. Gong, Phys. Rev. A **87**, 033807 (2013).
[11] K. Stannigel, P. Komar, S. J. M. Habraken, S. D. Bennett, M. D. Lukin, P. Zoller, and P. Rabl, Phys. Rev. Lett. **109**, 013603 (2012).
[12] S. S. Chen, H. Zhang, X. K. Song, F. G. Deng, H. B. Wang, and G. J. Yang, Ann. Phys. (Berlin) **530**, 1800239 (2018).
[13] S. E. Harris, Phys. Today **50**(7), 36 (1997).
[14] M. Fleischhauer, A. Imamoglu, and J. P. Marangos, Rev. Mod. Phys. **77**, 633 (2005).
[15] W. Stefan, R. Rémi, D. Samuel *et al.*, Science **330**, 1520 (2010).
[16] G. S. Agarwal and S. Huang, Phys. Rev. A **81**, 041803(R) (2010).
[17] A. H. Safavi-Naeini *et al.*, Nature (London) **472**, 69 (2011).
[18] V. Fiore, Y. Yang, M. C. Kuzyk, R. Barbour, L. Tian, and H. Wang, Phys. Rev. Lett. **107**, 133601 (2011).
[19] J. Q. Zhang, Y. Li, M. Feng, and Y. Xu, Phys. Rev. A **86**, 053806 (2012).
[20] K. Børkje, A. Nunnenkamp, J. D. Teufel, and S. M. Girvin, Phys. Rev. Lett. **111**, 053603 (2013).
[21] Y.-P. Gao, T.-J. Wang, C. Cao, S.-C. Mi, D. Yang, Y. Zhang, and C. Wang, IEEE Photonics J. **9**, 6800411 (2017).
[22] F. M. Buters, F. Luna, M. J. Weaver, H. J. Eerkens, K. Heeck, S. de Man, and D. Bouwmeester, Opt. Express **25**, 12935 (2017).
[23] Y. Chang, T. Shi, Y. X. Liu, C. P. Sun, and F. Nori, Phys. Rev. A **83**, 063826 (2011).
[24] A. Kronwald and F. Marquardt, Phys. Rev. Lett. **111**, 133601 (2013).
[25] S. Shahidani, M. H. Naderi, and M. Soltanolkotabi, Phys. Rev. A **88**, 053813 (2013).
[26] P. C. Ma, J. Q. Zhang, Y. Xiao, M. Feng, and Z. M. Zhang, Phys. Rev. A **90**, 043825 (2014).

[27] H. Wang, X. Gu, Y. X. Liu, A. Miranowicz, and F. Nori, Phys. Rev. A **90**, 023817 (2014).
[28] F. C. Lei, M. Gao, C. G. Du, Q. L. Jing, and G. L. Long, Opt. Express **23**, 11508 (2015).
[29] K. C. Yellapragada, N. Pramanik, S. Singh, and P. A. Lakshmi, Phys. Rev. A **98**, 053822 (2018).
[30] F. Massel *et al.*, Nature (London) **480**, 351 (2011).
[31] M. Karuza, C. Biancofiore, M. Bawaj, C. Molinelli, M. Galassi, R. Natali, P. Tombesi, G. DiGiuseppe, and D. Vitali, Phys. Rev. A **88**, 013804 (2013).
[32] A. Nunnenkamp, V. Sudhir, A. K. Feofanov, A. Roulet, and T. J. Kippenberg, Phys. Rev. Lett. **113**, 023604 (2014).
[33] X. B. Yan, W. Z. Jia, Y. Li, J. H. Wu, X. L. Li, and H. W. Mu, Front. Phys. **10**, 351 (2015).
[34] T. Wang, Y. Q. Hu, C. G. Du, and G. L. Long, Opt. Express **27**, 7344 (2019).
[35] H. J. Carmichael, *Lecture Notes in Physics* (Springer-Verlag, Berlin, 1993), Vol. 18.
[36] S. Gröblacher, A. Trubarov, N. Prigge, and G. D. Cole, Nat. Commun. **6**, 7606 (2015).
[37] Q. Mu, X. Zhao, and T. Yu, Phys. Rev. A **94**, 012334 (2016).
[38] J. Cheng, W. Z. Zhang, L. Zhou, and W. Zhang, Sci. Rep. **6**, 23678 (2016).
[39] W. Z. Zhang, J. Cheng, W. D. Li, and L. Zhou, Phys. Rev. A **93**, 063853 (2016).
[40] W. Z. Zhang, Y. Han, B. Xiong, and L. Zhou, New J. Phys. **19**, 083022 (2017).
[41] C. Y. Xin, S. S. Meng, and Y. H. Zhou, Int. J. Theor. Phys. **57**, 1659 (2018).
[42] C. J. Myatt *et al.*, Nature (London) **403**, 269 (2000).
[43] B. H. Liu *et al.*, Nat. Phys. **7**, 931 (2011).
[44] Y. D. Wang and A. A. Clerk, Phys. Rev. Lett. **110**, 253601 (2013).
[45] A. Metelmann and A. A. Clerk, Phys. Rev. Lett. **112**, 133904 (2014).
[46] C. Meier and D. J. Tannor, J. Chem. Phys. **111**, 3365 (1999).
[47] Y. Tanimura, Phys. Rev. A **41**, 6676 (1990).
[48] D. F. Walls and G. J. Milburn, *Quantum Optics* (Springer-Verlag, Berlin, 1994); M. O. Scully and M. S. Zubairy, *Quantum Optics* (Cambridge University, Cambridge, England, 1997).
[49] A. J. Leggett, S. Chakravarty, A. T. Dorsey, P. A. Matthew Fisher, A. Garg, and W. Zwerger, Rev. Mod. Phys. **59**, 1 (1987).
[50] W. H. Press, B. P. Flannery, S. A. Teukolsky, and W. T. Vetterling, *Numerical Recipes* (Cambridge University, Cambridge, England, 1989).
[51] S. Gröblacher, K. Hammerer, M. Vanner, and M. Aspelmeyer, Nature (London) **460**, 724 (2009).
[52] B. Peng, S. K. Özdemir, W. J. Chen, F. Nori, and L. Yang, Nat. Commun. **5**, 5082 (2014).
[53] S. H. Autler and C. H. Townes, Phys. Rev. **100**, 703 (1955).